Summary

Two topics are addressed in this thesis: Photoredox catalyzed C–C bond formation and transition metal catalyzed C–N bond formation via metallonitrenoid intermediates. Both topics are briefly introduced in the **Introduction**. In photoredox catalysis, absorption of light brings a dye molecule into the excited state, which can be followed by (1) relaxation via luminescence or non-radiative processes back to the ground state, (2) energy transfer, or (3) reactive single electron redox processes between the excited state photocatalyst (dye) and the substrates. The latter reactions are the domain of photoredox catalysis. Such single electron transfer processes typically involve the longer-lived triplet excited state of the photocatalyst and enable controlled formation of radical species that undergo propagation mechanisms. Termination can either involve the catalyst or radical-radical coupling/ disproportionation reactions. Although organic photosensitizers (or dyes) and photosensitizers that are based on first row transition metals are developed for photoredox catalysis, the use of noble metal-based photoredox catalysts (in particular iridium catalysts) is still popular and under development (see also Chapter 1 and 2). Three illustrative examples of C–C bond formation reactions proceeding via photoredox catalysis are discussed in the Introduction.

The second topic addressed in this thesis involves C–N bond formation reactions via reactive metallonitrenoid intermediates. Transition metal complexes can enable selective nitrene transfer reactions, via metallonitrenoid intermediates, for C–N bond formation reactions. These reactions can be performed under mild conditions and can be more selective than other C–N bond forming reactions. Isolation of metallonitrenoid species is non-trivial and only recently Betley and coworkers have isolated such complexes. Reactions that include reactive metallonitrenoid intermediates are more common, and two illustrative examples of C–N bond formation reactions proceeding via metallonitrenoid intermediates are introduced in some detail in the Introduction: Pyrrolidine formation via C–H amination and aziridination reactions. Chapters 3, 4 and 5 continue on these developments.

In **Chapter 1** a new cationic iridium-based photosensitizer was developed containing two chromenopyridinone (Chp) ligands and one di-*tert*-butylbipyridine (dtbbpy) ligand (Figure 1). The lowest unoccupied molecular orbital (LUMO) is located at the bipyridine ligand and is therefore similar in energy as in the frequently applied photocatalyst $[Ir(ppy)_2(dtbbpy)]^+$, where ppy is 2-phenylpyridinyl. The electron withdrawing character of the ester moiety lowers the highest occupied molecular orbital (HOMO), located at the metal center and at the phenyl ring of the ligand, compared to $[Ir(ppy)_2(dtbbpy)]^+$. A larger HOMO-LUMO gap results in a larger range of redox strength that can be achieved for $[Ir(Chp)_2(dtbbpy)]^+$. The difference of the HOMO-LUMO gap between $[Ir(Chp)_2(dtbbpy)]^+$ and $[Ir(ppy)_2(dtbbpy)]^+$ was measured as a shorter luminescence wave length for the former. The excited state of $[Ir(Chp)_2(dtbbpy)]^+$, with a lifetime of 0.5 µs, was studied by pump–probe X-ray absorption near edge structure (XANES) spectroscopy and DFT calculations. The rigid

structure of the complex hardly changes in the excited state, with metal-ligand bond length changes of less than 0.01 Å. The change in electronic structure from the ground state to the excited state is visualized in the transient spectrum (Figure 2). Metal-to-ligand charge transfer in its excited state results in a larger energy change for the 2p orbitals than for the e_g orbitals, resulting in a white band shift to higher energy (from B to B'). The excited state also contains a hole in a t_{2g} orbital, to which an electron could be excited, leading to an additional absorption peak at lower energy (A').

Figure 1. The structure of the $[Ir(Chp)_2(dtbbpy)]PF_6$ complex.

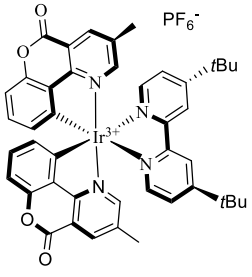

Figure 2. The (experimental and calculated) XANES spectrum of $[Ir(Chp)_2(dtbbpy)]PF_6$ in MeCN and a transient XANES spectrum of its excited state, with an energy level diagram of some important molecular orbitals which are relevant to explain the transient XANES spectra.

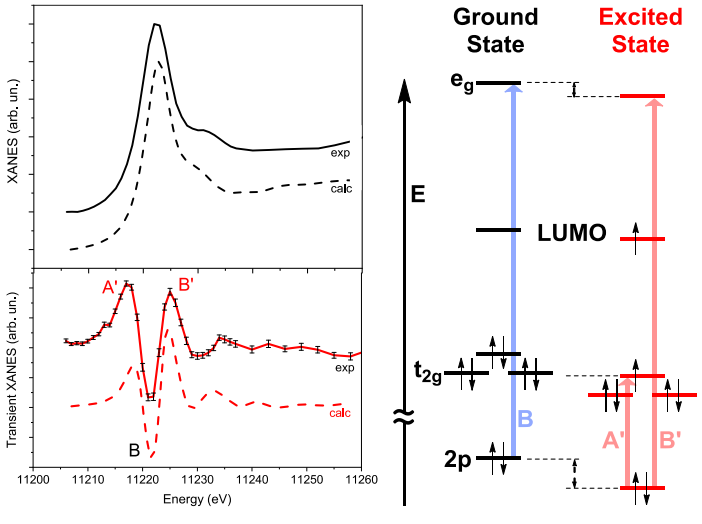

In **Chapter 2** we describe our efforts to use photoredox catalysis to activate monochloroacetic acid for organic synthesis applications. Photoredox catalysis is a useful method for the formation of new C–C bonds and monochloroacetic acid (MCAA) is a useful starting material that is widely used in industry. Most transformations involving MCAA are based on nucleophilic substitution. Generation of a radical intermediate could lead to new synthetic applications of MCAA and

therefore we aimed at using MCAA in photoredox catalysis in a reaction with styrene and related substrates. The photochemical reaction of olefins with iodoacetic acid and bromoacetic acid are well documented and easier, but the stronger C–halide bond in MCAA is more challenging to break. Under excitation by blue light, the neutral photoredox catalyst *fac*-[Ir(ppy)$_3$] could reduce the C–Cl bond to generate a carboxymethanide radical under mild reaction conditions. Via this method, γphenyl-γ butyrolactone can be formed by cyclization and 4-chloro-4-phenylbutanoic acid can be formed via chloroalkylation (Scheme 1). Selective formation of the two desired products was observed (albeit in moderate yields). Over time the catalyst precipitates from solution as a cation or in a decomposed form. For the organic photoredox catalyst *N,N*-5,10-di(2-naphthalene)-5,10-dihydrophenazine, the precipitate was identified by mass and EPR spectroscopy as the cation of the catalyst. In an attempt to trap a radical intermediate during the reaction with TEMPO, LC-MS analysis of the formed product indicated the formation of a chloromethyl radical (Scheme 2), but efforts to apply this decarboxylative formation of a chloromethyl radical from MCAA in cyclopropanation reactions were unsuccessful.

Scheme 1. The photoredox catalyzed reaction between monochloroacetic acid and styrene.

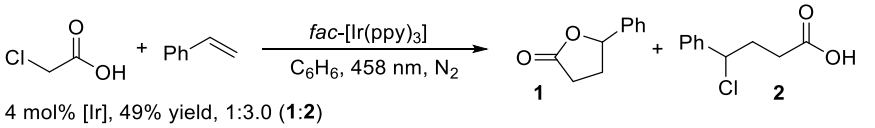

4 mol% [Ir], 49% yield, 1:3.0 (**1**:**2**)
10 mol% [Ir], 84% yield, 1:4.3 (**1**:**2**)

Scheme 2. The photoredox formation of 1-(chloromethoxy)-2,2,6,6-tetramethyl-piperidine.

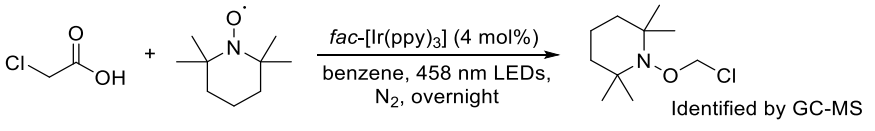

Nitrene transfer reactions are another type of efficient bond formation. Generally, nitrene transfer reactions are performed with azides or iminoiodinanes, but for acyl nitrene transfer, preparation and storage of such precursors is troublesome. The use of 1,3,4-dioxazol-2-one derivatives (dioxazolones) as acyl nitrene precursors in directed C–H amidation reactions triggered us to study this substrate group for their application in new C–N bond formation reactions. **Chapter 3** provides an overview of the development of dioxazolones as efficient nitrene transfer reagents in catalysis since 2012. Directed C–H amidation reactions are a major part of this development. Various directing groups have been used and C–H groups of aryl, alkyl or olefins are successfully amidated. Aryldioxazolones have even been applied as a directing group for C–H alkylation and subsequent amidation. Dioxazolones could also be used in allylic amidation reactions or in intramolecular C–H amidation reactions to form

lactam products. Addition reactions on styrene or phenylacetylene have been reported for the formation of oxazolines or oxazoles.

In Chapters 4 and 5, we demonstrate our efforts to develop a new synthetic method to convert dioxazolones in a selective C–N bond forming reaction leading to formation of *N*-acyl amidines. Direct methods for the synthesis of amidines are desired, as they are present in organometallic complexes and in many biologically active compounds. Synthetic methods for the formation of *N*-acyl amidines are particularly important, as they can be used as starting material for the synthesis of a variety of heterocyclic compounds.

In **Chapter 4**, we report a new copper catalyzed 3-component reaction for the formation of *N*-acyl amidines with terminal alkynes, dioxazolones and secondary amines (Scheme 3). Xantphos copper acetate [Cu(OAc)(Xantphos)] was found to be the most efficient catalyst for these transformations. Even in air, the use of only 5 mol% of catalyst led to quantitative formation of the products within 10 minutes. Under an inert atmosphere, the catalyst loading could even be lowered to 2 mol% to obtain high yields (94%). Lower yield of the product under non-optimized reaction conditions was generally accompanied with isocyanate formation via the Curtius rearrangement. Although aliphatic terminal alkynes do not work for the formation of *N*-acyl amidines, product formation from ethylenes 3-ethynylpyridine and 3-ethynylthiophene was very efficient. Primary and smaller secondary amines do not work, as coordination of these substrates leads to catalyst poisoning, but if the bulk of the amine inhibits its coordination to the metal, dioxazolones can be activated and high yields for product formation can be obtained. For the transformation of 3-phenyl-1,4,2-dioxazol-5-one derivatives, [Cu(OAc)(Xantphos)] does not work as the catalyst. However, 10 mol% of CuI salt can catalyze formation of the desired products in moderate to good yields.

Scheme 3. The copper catalyzed 3-component reaction of 1,4,2-dioxazol-5-ones to *N*-acyl-amidines.

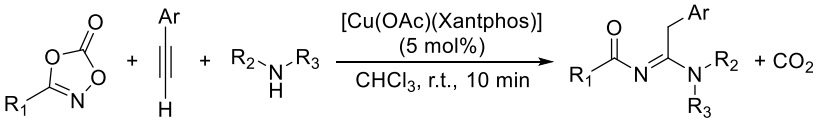

To get more insights into the new 3-component reaction, we performed the mechanistic study described in **Chapter 5**. Key steps in the mechanism of this reaction are shown in Scheme 4. Although H/D-scrambling in ^{1}H-NMR spectroscopy showed a reversible formation of Xantphos copper acetylide [Cu(CCPh)(Xantphos)] from [Cu(OAc)(Xantphos)] in absence of amine, ^{31}P NMR studies showed that the amine was necessary to push the equilibrium effectively to [Cu(CCPh)(Xantphos)]. The acetate ligand plays an important role in the catalytic cycle, which is supported by a faster reaction rate for [Cu(OAc)(Xantphos)] compared to [Cu(NCMe)$_2$(Xantphos)](BF$_4$). A crystal structure of [Cu(OAc)(Xantphos)(HCCPh)] was obtained, showing binding interactions of the acetate ligand to the C(sp)–H bond of phenylacetylene (Figure 3). Reaction rates obtained by *in situ* pressure analysis in a closed vessel gave further

insights into the mechanism. A first order in both the [catalyst] and the [dioxazolone], combined with saturation kinetics for the [phenylacetylene] and the results of deuteration studies, revealed that the dioxazolone activation by the Cu^{I}-acetylide complex [Cu(CCPh)(Xantphos)] is the rate determining step, which is preceded by a fast pre-equilibrium between [Cu(OAc)(Xantphos)] and [Cu(CCPh)(Xantphos)]. DFT analysis of the proposed intermediates supports this and reveals an energy barrier of ~20 kcal mol^{-1} for dioxazolone activation resulting in formation of a copper *N*-acyl nitrene intermediate (Scheme 4). Subsequent nitrene insertion into the Cu–C bond of the acetylide moiety and capture of the amine substrate result in formation of the final *N*-acyl amidine product, which are fast steps following the rate determining dioxazolone activation step. This is confirmed by the zero-order reaction kinetics in the [amine]. Isocyanate formation via the Curtius rearrangement, which is the main side reaction, was calculated to have a slightly higher energy barrier than nitrene insertion into the Cu–C bond, which is in line with the experimental observations.

Scheme 4. Key steps in the mechanism of the copper catalyzed three component reaction of 1,4,2-dioxazol-5-ones to *N*-acyl-amidines.

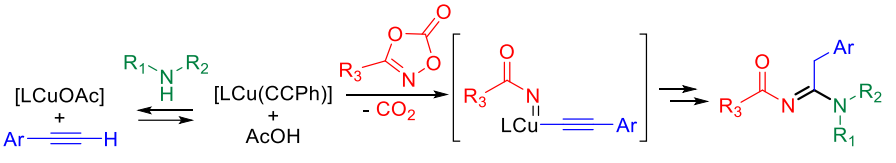

Figure 3. The crystal structure obtained by crystallization in the presence of acetylene, showing a H-bonding interaction with the acetate.